2011 50th IEEE Conference on Decision and Control and
European Control Conference (CDC-ECC)
Orlando, FL, USA, December 12-15, 2011

Modeling Cyclic Dispersion in Autoignition Combustion

Erik Hellström and Anna G. Stefanopoulou
Department of Mechanical Engineering
University of Michigan
{erikhe,annastef}@umich.edu

Abstract— **A two-state discrete-time model is developed for the cycle-to-cycle dynamics in lean-fueled controlled autoignition engines. The main goal is to capture the cyclic variability in the combustion phasing which is a key performance variable in combustion control. The model is physics based, the states are the temperature and the fuel mass at intake valve closing, and simple enough so it may provide insights into the dynamics and causes of the behavior. The parameters are crudely calibrated using data that include late phasing approaching to misfire and the model captures the important effect of heat release during the re-compression of the residual gas. The model is shown to predict the coupling between cycles in the sense that, when driven by a stochastic input, the model reproduces the evolution and the magnitude of the cyclic variability with similar statistical properties to measured data.**

I. Introduction

It was early noted that controlled autoignition (CAI) combustion, also known as homogeneous charge compression ignition (HCCI) combustion, can have low cyclic variability (CV) compared to spark ignited (SI) combustion [1], [2]. However, at certain operating conditions HCCI combustion phasing can instead be oscillatory or unstable. The CAI combustion is induced and sustained by raising the charge temperature of the next cycle by trapping and re-compressing (recycling) residual gases from the earlier cycles [3]. The HCCI process is extremely efficient with very low emissions but can exhibit significant oscillations at late phasing and runaway-knock phenomena at high loads [4]–[7]. This behavior indicates that there is significant nonlinear feedback between cycles that can stabilize or destabilize the process. The coupling is generally attributed to combustion inefficiency and temperature effects such as the temperature of the residual gases or cylinder walls [8]–[11].

The described characteristics impose limits on the achievable operating range in the absence of control that can reduce the CV. Even if a switch from HCCI to SI is deemed necessary, precise control of the transition is needed [12]. This transition process can have complex behavior as shown in the experiments and analysis by Daw et al. [9], [13]. Therefore, to enable control strategies for achieving low variability or mode switching it is vital to understand the dominant controllable mechanisms of this process and to describe them with low-order models. Further, published experimental results and data analysis [8], [9], [14] indicate that there may be simple deterministic features that can capture the main trends of the behavior.

To this end, we develop a two-state cycle-discrete model of the dynamics of the mean gas temperature and the amount of unburned fuel that are recycled from previous cycles through an early closing of the exhaust valve [3], also known as negative valve overlap (nvo) strategy. The novelties of this modeling approach are the low order and that a state-dependent combustion efficiency is estimated from measurements and included in the model. For operating regimes with low variability, where the unburned fuel is a negligible concern, HCCI combustion models have been developed with a few lumped states (see, e.g., [15]–[17]) or with higher fidelity (in, e.g., [18], [19]). Misfire in HCCI is studied in simulation using models including chemical kinetics and gas flows in [20] and using a simplified eight state model in [21]. A one-state control model was developed in [22] and analysis of the stability of HCCI with large amounts of residual gas was shown in [23]. The nonlinear coupling between combustion phasing and the residual temperature allowed the prediction of unstable behavior with limit cycles at late phasing and runaway knock at early phasing. Similar analysis is shown in [24].

This paper extends these works by including a second dynamic state, the unburned fuel amount, in addition to a charge temperature state. The focus here is on the coupling between cycles introduced by temperature of the residuals and the amount of unburned fuel. The cylinder wall temperature has also a significant effect on the process [7] but it is reasonable to expect that it varies slower. Measurements of wall temperature by Wilhelmsson et al. [25] show rise times in the order of 100 sec in load transients (e.g., at an engine speed of 2000 rpm there are about 17 cycles per second). Furthermore, the conditions studied here typically have a residual gas fraction above 40% which could easily dominate the temperature coupling between two consecutive cycles and thus present a more challenging controls task.

With respect to the high amount of recycled charge, the re-compression strategy bears similarities to the operation of two-stroke engines and it is interesting to note that similar cyclic behavior seen in two-stroke applications [5] also has been reported from four-stroke engines [8]. Another process where feedback from the residual gas plays an important role is in lean operation of conventional SI engines. Although the fraction of residual gas in SI is typically lower than in HCCI, the coupling between cycles can give high CV. For this case, Daw et al. [26] successfully modeled the dynamics by using a two-state nonlinear model with parametric uncertainties modeled as stochastic noise. Although this process is clearly

978-1-61284-799-3/11/$26.00 ©2011 IEEE

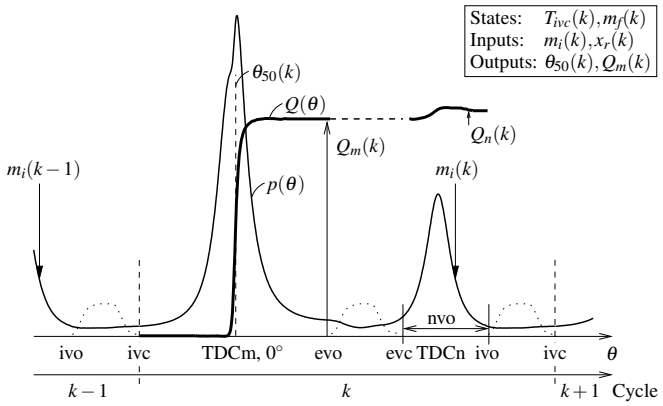

Fig. 1. Definition of the engine cycle and important variables for typical cylinder pressure $p(\theta)$, heat release $Q(\theta)$, and valve lift (dotted line).

distinct from HCCI, our approach to capture the dynamics is similar. Our aim is to find a low-order description of the main features in observed data. For this, we lump complex effects that are not modeled into one stochastic input to the simple model. Specifically, the fluctuations of the residual gas fraction is modeled by Gaussian white noise.

The paper is organized as follows. First the experimental setup is described, an overview of the studied dynamical system is given, and some observations on CV are made from the experiments. After that, the model is derived and parametrized. Finally, the agreement between model predictions and measured data are shown, and conclusions from the work is drawn.

II. System overview and experimental observations of cyclic phenomena

The combustion cycle can be divided into breathing and combustion phases where the main combustion occurs in the period between the intake valve closing and the exhaust valve opening. For controlled autoignition, combustion may also occur during the period with nvo. These three phases, breathing, main combustion, and nvo combustion, from a typical engine cycle are shown together with the definition of important events and variables in Fig. 1.

The proposed model captures the evolution of the gas temperature and the fuel mass, as shown in the block diagram in Fig. 2, because combustion phasing is determined primarily by temperature [27] and the amount of unburned fuel is included to capture incomplete combustion during late phasing. The inputs of the model in Fig. 2 are injected fuel mass m_i and residual gas fraction x_r which is regulated through valve control. The outputs considered are the 50% burn angle θ_{50} and the gross heat release during main combustion Q_m. The states are the temperature and fuel mass, denoted by T_{ivc} and m_f respectively, at the beginning of the cycle defined at intake valve closing (ivc). The other variables in Fig. 2 are the temperature T_{evc} at exhaust valve closing (evc), the residual gas temperature T_r, the unburned fuel m_{mu} after main combustion, and the unburned fuel m_{nu} after nvo combustion.

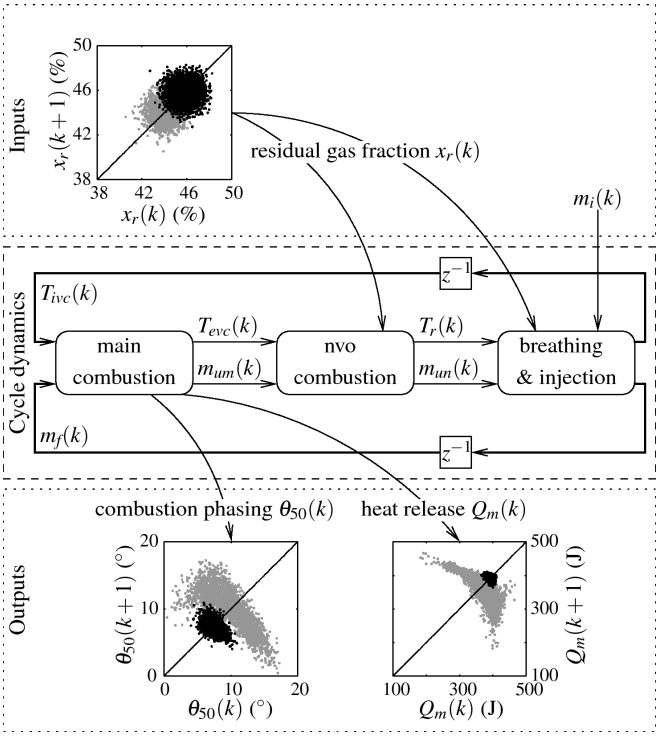

Fig. 2. Block diagram for the combustion cycle dynamics showing the combustion and breathing phases, the inputs, and the outputs. Also shown are the experimental return maps for the inputs and outputs for one case with high CV (gray dots) and one case with lower CV (black dots).

Figure 2 also shows experimental data from two different operating conditions. The experimental results were obtained from a 0.55 L single-cylinder gasoline engine, installed and operated at the Automotive Laboratory at the University of Michigan as detailed in [28]. In-cylinder pressure were sampled each crank angle degree and 3000 consecutive cycles were recorded at each operating point. Nominal operating conditions for the experiments were 2000 rpm controlled by a hydraulic dynamometer and the coolant temperature was controlled at 90°C. The injected fuel mass m_i was kept constant at about 9.6 mg/cycle corresponding to 2.8 bar net IMEP. The engine is equipped with an electro-hydraulic fully-flexible valve actuation system which allows control of lift, timing, and duration of each valve event to be controlled independently. The return maps in Fig. 2 show the relationship between two subsequent values of the variables and are acquired with the valve timings set at two different settings. These settings affect the mean value of x_r from 46% (black dots) to 44% (gray dots). The successive cycle-to-cycle values of x_r are assumed uncorrelated in both cases, as indicated by the return maps for x_r in Fig. 2. However, the relationship between successive cycle-to-cycle values of the outputs change notably when reducing the mean x_r. As seen in Fig. 2, the experimental output for the low CV case (black dots) do not show any strong correlation whereas in the high CV case (gray dots) characteristic shapes appear in the return maps which indicate deterministic couplings between consecutive cycles. These characteristics are typical

for our experimental findings and they get more pronounced as the CV increases.

From the experimental results in Fig. 2 it is seen that a bifurcation occur when reducing x_r where the term bifurcation is used in the general sense meaning that the dynamical behavior changes qualitatively. Our two-state model captures the nonlinear feedback between cycles and predicts the main features in observed data as shown in Sec. V.

III. Combustion model

A natural choice of model states of a low-order model are the temperature $T_{ivc}(k)$ at intake valve closing and the fuel amount $m_f(k)$ in the beginning of cycle k. The definition of the cycle and important variables in the model are shown in Fig. 1.

In the following sections, the two-state model is derived. First the modeling of the heat release and fuel dynamics are covered which are the parts that distinguish this model from related work (such as [15]–[17], [22]–[24]).

A. Heat release

The crank angle timing θ_m of the main combustion is given by an Arrhenius expression whereas the timing θ_n for the combustion during re-compression is constant. The ignition delay for the main combustion is given by

$$\tau = Ap(\theta)^n \exp\big(B/T(\theta)\big) \tag{1}$$

with the tuned parameters (A,B,n) [29]. The pressure $p(\theta)$ and temperature $T(\theta)$ are given in Sec. III-C. The start of combustion θ_{soc} is then found from

$$1 = \int_{\theta_{ivc}}^{\theta_{soc}} \frac{dt}{\tau}, \quad dt = d\theta/\omega \tag{2}$$

where ω is the engine speed. Finally, the end of the main combustion θ_m is given by

$$\theta_m = \theta_{soc} + \Delta\theta, \quad \Delta\theta = d_1\theta_{soc} + d_2 \tag{3}$$

where $\Delta\theta$ is the burn duration and (d_1,d_2) are tuned parameters. When tuning the parameters (A,B,n,d_1,d_2) to experimental data, start of combustion θ_{soc} is interpreted as the 10% burn angle and θ_m as the 90% burn angle. The combustion phasing, the 50% burn angle, is given by

$$\theta_{50} = \theta_m + \Delta\theta/2. \tag{4}$$

Both combustion events are adiabatic constant-volume processes and the temperature rises are

$$\Delta T_m = \frac{Q_{nm}}{c_v m_t}, \quad \Delta T_n = \frac{Q_{nn}}{c_v m_t x_r} \tag{5}$$

where m_t is the charge mass, given later in Eq. (18), and $m_t x_r$ is the residual charge mass. Assuming that sufficient oxygen is present (lean combustion), the net heat of reaction during main combustion Q_{nm} is modeled by

$$Q_{nm} = m_f \eta_m(\theta_m) q_m \tag{6}$$

where m_f is the fuel mass, η_m is the combustion efficiency, and $q_m = q_{lhv}(1-\varepsilon_c)$ where q_{lhv} is the lower heating value and ε_c represents heat losses. The fraction x_r of the unburned fuel after the main combustion $m_f(1-\eta_m(\theta_m))$ gives the net heat release during the nvo period (see Fig. 1) Q_{nn} as

$$Q_{nn} = m_f(1-\eta_m(\theta_m))x_r\eta_n q_n \tag{7}$$

where $q_n = q_{lhv}(1-\varepsilon_r)$ and η_n is the combustion efficiency of the re-compression phase. The combustion efficiencies $\eta_m(\theta_m)$ and η_n are estimated in Sec. IV.

B. Fuel dynamics

The main combustion consumes a fraction $\eta_m(\theta_m)$ of the fuel mass and after the exhaust a fraction x_r of the residual gases is trapped. During the nvo period, a fraction η_n is further consumed. With homogeneous residuals, the unburned fuel amounts (m_{um}, m_{un}) after main and nvo combustion, respectively, are

$$m_{um}(k) = m_f(k)\,(1-\eta_m(\theta_m)) \tag{8}$$

$$m_{un}(k) = m_{um}(k)x_r(k)\,(1-\eta_n) \tag{9}$$

where $\theta_m = \theta_m(T_{ivc}(k))$ is given by (1)–(3). The fuel mass in the beginning of the next cycle is then simply

$$m_f(k+1) = m_i(k) + x_r(k)\,(1-\eta_m(\theta_m))\,(1-\eta_n)\,m_f(k) \tag{10}$$

where $m_i(k)$ is the injected fuel mass.

C. Temperature dynamics

By assuming adiabatic mixing of ideal gases with constant specific heats, the temperature at intake valve closing $T_{ivc}(k+1)$ of cycle $k+1$ is given by

$$T_{ivc}(k+1) = (1-x_r(k))T_{im} + x_r(k)T_r(k) \tag{11}$$

where $x_r(k)$ is the residual gas fraction and T_{im} is the intake manifold temperature which is considered known but is typically close to ambient temperature. The temperature of the residual gas $T_r(k)$ of cycle k is derived in the following.

The compression and expansion are polytropic processes with slope γ. The pressure and temperature are thus given as a function of crank angle θ by

$$\left.\begin{aligned} p(\theta) &= p_{ivc}\left(\frac{V_{ivc}}{V(\theta)}\right)^{\gamma} \\ T(\theta) &= T_{ivc}\left(\frac{V_{ivc}}{V(\theta)}\right)^{\gamma-1} \end{aligned}\right\} \text{ if } \theta \in (\theta_{ivc}, \theta_m] \tag{12a}$$

$$\left.\begin{aligned} p(\theta) &= p_{am}\left(\frac{V(\theta_m)}{V(\theta)}\right)^{\gamma} \\ T(\theta) &= T_{am}\left(\frac{V(\theta_m)}{V(\theta)}\right)^{\gamma-1} \end{aligned}\right\} \text{ if } \theta \in (\theta_m, \theta_{evo}] \tag{12b}$$

where $V(\theta)$ is the cylinder volume function and $V_x = V(\theta_x)$ is the volume at the crank angle θ_x. It is assumed that the combustion occurs instantaneously at θ_m and the state after combustion is given by

$$T_{am} = T(\theta_m) + \Delta T_c, \quad p_{am} = p(\theta_m)\frac{T_{am}}{T(\theta_m)} \tag{13}$$

where ΔT_c is given by (5).

The blowdown occurs instantaneously and the remaining gases follow a polytropic process from pressure at exhaust valve opening $p(\theta_{evo})$ to exhaust manifold pressure p_{em},

$$T_{bd} = T_{evo}\left(\frac{p_{em}}{p(\theta_{evo})}\right)^{1-1/\gamma}. \tag{14}$$

The temperature of the residual gases at exhaust valve closing is

$$T_{evc} = c_e T_{bd} \tag{15}$$

where c_e accounts for cooling of the residuals during the exhaust process.

The compression and expansion during nvo are polytropic processes, thus $p(\theta)$ and $T(\theta)$ are given by expressions analogous to Eq. (12a) for $\theta \in (\theta_{evc}, \theta_n]$ and Eq. (12b) for $\theta \in (\theta_n, \theta_{ivo}]$. The state, after instantaneous combustion of the unburned fuel at θ_n, is given by

$$T_{an} = T(\theta_n) + \Delta T_r, \quad p_{an} = p(\theta_n)\frac{T_{an}}{T(\theta_n)} \tag{16}$$

where ΔT_r is given by (5). Finally, the temperature of the residual gases at intake valve opening is formulated based on the temperature T_{ivo} obtained after polytropic expansion from T_{an}:

$$T_r = T_{ivo} = T_{an}\left(\frac{V(\theta_n)}{V_{ivo}}\right)^{\gamma-1} \tag{17}$$

Now, express the charge mass as

$$m_t = \frac{p_{ivc}V_{ivc}}{RT_{ivc}} \tag{18}$$

and introduce the following parameters

$$\alpha = c_e\left(\frac{p_{em}}{p_{ivc}}\right)^{\frac{\gamma-1}{\gamma}}\left(\frac{V_{evc}}{V_{ivo}}\right)^{\gamma-1} \tag{19a}$$

$$\beta = \frac{q_m(\gamma-1)}{p_{ivc}V_{ivc}^{\gamma}} \tag{19b}$$

$$\zeta = \frac{q_n\eta_n(\gamma-1)}{p_{ivc}V_{ivc}V_{ivo}^{\gamma-1}}V(\theta_n)^{\gamma-1} \tag{19c}$$

that are assumed constant for a given operating condition. By combining Eq. (5)–(7) and (12)–(18) this parametrization gives the following description for the temperature of the residual gases at the end of cycle k:

$$T_r(k) = \Big\{\alpha\left[1+\beta\eta_m(\theta_m)m_f(k)V(\theta_m)^{\gamma-1}\right]^{\frac{1}{\gamma}} + \zeta m_f(k)(1-\eta_m(\theta_m))\Big\}T_{ivc}(k) \tag{20}$$

where $\theta_m = \theta_m(T_{ivc}(k))$ is given by (1)–(3). The parameter α is related to the blowdown and exhaust process (note that $V_{evc}/V_{ivo} \approx 1$ since nvo typically is close to symmetrical). The β and ζ are related to the temperature rise per mass of fuel that burns during the main combustion and during the re-compression, respectively.

D. Complete model

The temperature at ivc and the fuel mass in the next cycle $k+1$ are given by the states at cycle k and the inputs, $m_i(k)$ and $x_r(k)$,

$$\begin{cases} T_{ivc}(k+1) = f\left(T_{ivc}(k), m_f(k), x_r(k)\right) \\ m_f(k+1) = g\left(T_{ivc}(k), m_f(k), m_i(k), x_r(k)\right) \end{cases} \tag{21}$$

where f is defined by (11), (20) and g is defined by (10). In the comparison with measurements, we will focus on the following outputs

$$\begin{cases} \theta_{50}(k) = h(T_{ivc}(k)) \\ Q_m(k) = m_f(k)q_{lhv}\eta_m(\theta_m(T_{ivc}(k))) \end{cases} \tag{22}$$

given by (1)–(4) and the efficiency (24) given in Sec. IV. Compared to related work (such as [15]–[17], [22]–[24]) the state-dependent efficiency $\eta_m(\theta_m(T_{ivc}(k)))$, the term with the parameter ζ, and the parameter η_n in Eq. (10) and (20) are the important differences since these represent the effect of incomplete combustion, heat release during re-compression, and recycled unburned fuel. In particular, the one-state model in [22] is obtained by setting $\eta_m = \eta_n = 1$, $\zeta = 0$, and $V_{evc}/V_{ivo} = 1$.

The model above is based on fundamental physics but represents a considerable simplification of the complex phenomena in the combustion process. All these higher order dynamical effects combined are here treated as stochastic perturbations of the model. Specifically, the input x_r is modeled as a constant $\bar{x}_r$ with added Gaussian white noise,

$$x_r(k) = \bar{x}_r + e(k), \quad e(k) \in N(0,\sigma) \tag{23}$$

where $e(k)$ is normally distributed with zero mean and variance σ^2.

IV. Parametrization

In order to analyze the measurements and to determine model parameters, the data are processed by an iterative procedure to produce estimates of important variables for each individual cycle. This procedure includes residual gas fraction estimation, gross heat release analysis, and estimation of unburned fuel and combustion efficiencies. The results from the analysis are summarized below.

The model of the combustion efficiency $\eta_m(\theta_m)$ is shown in Fig. 3 together with a curve fit using the function

$$\eta_m(\theta) = e_1\left[1+\exp\left(\frac{\theta-e_2}{e_3}\right)\right]^{-1} \tag{24}$$

which captures the mean of the experimentally calculated values. The model captures the expected qualitative dependence on combustion timing. However, our model does not capture yet quantitative aspects such as peak combustion efficiency, the combustion timing where the efficiency starts to drop, and the rate with which the efficiency drops. These features are expected to vary and primarily depend on equivalence ratio and engine speed [30].

The temperature parameters α and β were computed from (19a) and (19b) respectively, whereas ζ was increased from

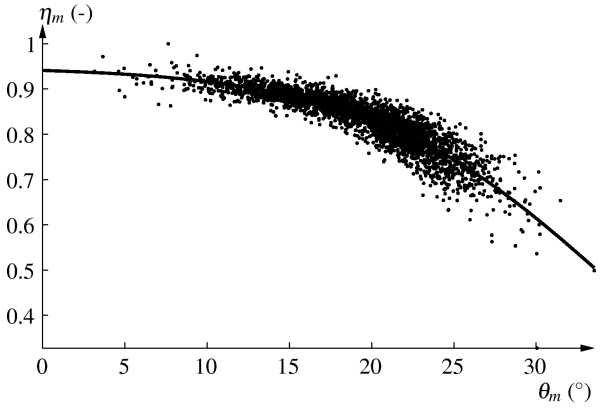

Fig. 3. Combustion efficiency estimation.

its nominal value manually in order to roughly tune the predicted onset of oscillations to match the measured data.

When the model given by (21)–(22) is fully parametrized, it can be simulated given initial conditions $T_{ivc}(0), m_f(0)$ and inputs. The injected fuel mass $m_i(k)$ is kept at the constant value used in the experiments and residual gas fraction x_r is chosen from Eq. (23). The mean $\hat{x}_r$ and variance σ^2 of the residual gas fraction are estimated from combustion analysis results of the measurements. These show that $\hat{x}_r$ is proportional to nvo and that σ is about 0.8% in all cases.

V. Model evaluation

Model predictions for varying nvo are generated by feeding the model (21) with $x_r(k)$ sampled from a normal distribution with standard deviation $\sigma = 0.8\%$ and different means $\bar{x}_r$. In the evaluation, the initial conditions $T_{ivc}(0), m_f(0)$ for the model are guessed. The model is then iterated a large number of times (or until convergence) and the initial transients are removed.

The agreement between the predicted and measured value of the 50% burn angle $\theta_{50}(k)$ in (22) is shown in Fig. 4. The predicted and measured total heat release $Q_m(k)$ in (22) are compared in Fig. 5. The thickness of the predicted heat release return map is smaller than in the measurements. One way to capture the observed dispersion better is to include the observed variability seen in Fig. 3 in our combustion efficiency model (24) along with the mean value. Still, the basic trends and patterns are predicted well when gradually proceeding from a low to a high variability case by decreasing the nvo and thereby the mean residual gas fraction. The different directions, or "legs", that appear in the return maps are getting more pronounced as x_r decreases.

VI. Conclusions

A nonlinear model with two states is developed for the cycle-to-cycle dynamics of lean HCCI combustion. The model is based on fundamental physics and the states are the temperature and the fuel amount in the beginning of the cycle since these are assumed to be the two most important variables for this case. Higher order dynamical effects that are not modeled are accounted for by perturbing

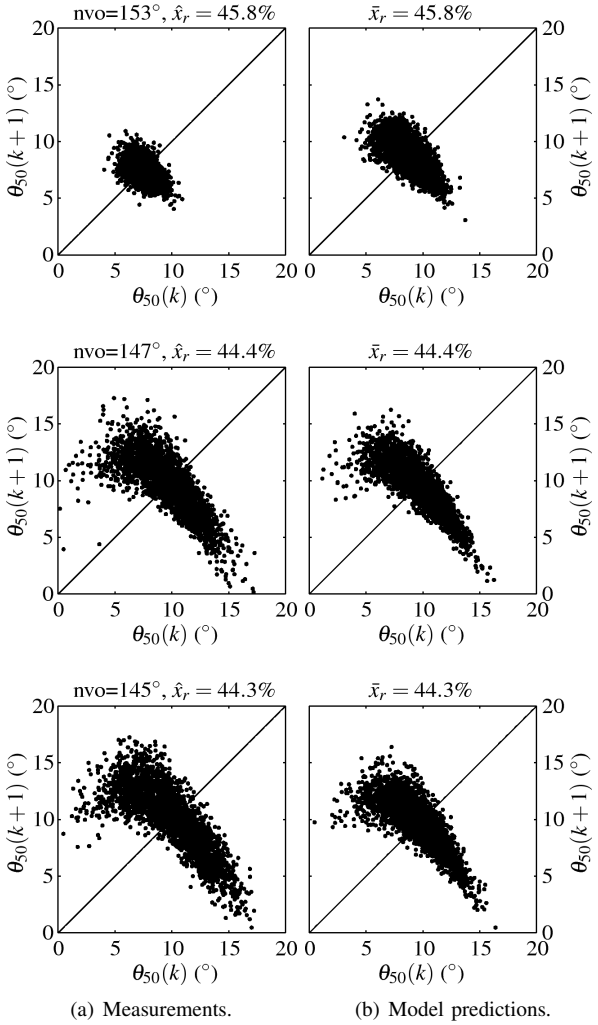

(a) Measurements. (b) Model predictions.

Fig. 4. Return maps for the 50% burn angle $\theta_{50}(k)$.

the residual gas fraction with Gaussian white noise. The result is a deterministic nonlinear model that, when driven with stochastic input, reproduces the evolution and the magnitude of the CV with statistical properties similar to measured data. Specifically, this is shown in the comparisons between model predictions and measured data of combustion phasing and heat release where the basic trends are in good agreement.

The developed low-order model captures the main features and can, e.g, be used for developing cycle-resolved controls aiming at reducing variability. The model is simple and based on physics and may therefore be useful in providing insights into the dynamical behavior in conditions with high CV.

Acknowledgments

Jiří Vávra and Laura Manofsky are thanked for their invaluable efforts acquiring the measurements. For helpful discussions on cyclic variability, we thank C. Stuart Daw at Oak Ridge National Laboratory and John W. Hoard at the University of Michigan.

This material is based upon work supported by the Department of Energy (National Energy Technology Laboratory) under award number DE-EE0003533.

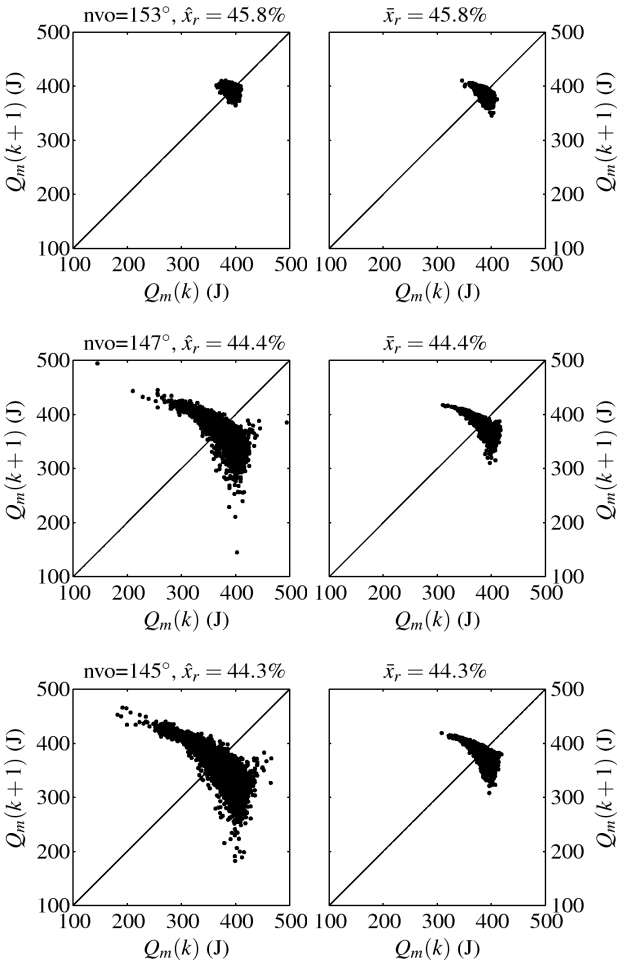

(a) Measurements. (b) Model predictions.

Fig. 5. Return maps for the heat release $Q_m(k)$ during main combustion.

REFERENCES

[1] S. Onishi, S.H. Jo, K. Shoda, P.D. Jo, and S. Kato. Active thermo-atmosphere combustion ATAC–a new combustion process for internal combustion engines. In *Automotive Engineering Congress and Exposition*, 1979. SAE 790501.

[2] D. Law, D. Kemp, J. Allen, G. Kirkpatrick, and T. Copland. Controlled combustion in an IC-engine with a fully variable valvetrain. In *SAE World Congress*, 2001. SAE 2001-01-0251.

[3] J. Willand, R-G. Nieberding, G. Vent, and C. Enderle. The knocking syndrome–its cure and its potential. In *SAE Int. Fall Fuels and Lubricants Meeting and Exhibition*, 1998. SAE 982483.

[4] R.H. Thring. Homogeneous charge compression ignition (HCCI) engines. In *SAE Int. Fall Fuels and Lubricants Meeting and Exhibition*, 1989. SAE 892068.

[5] Y. Ishibashi and M. Asai. Improving the exhaust emissions of two-stroke engines by applying the activated radical combustion. In *SAE Int. Congress and Exposition*, 1996. SAE 960742.

[6] L. Koopmans and I. Denbratt. A four stroke camless engine, operated in homogeneous charge compression ignition mode with commercial gasoline. In *SAE World Congress*, 2001. SAE 2001-01-3610.

[7] J.-O. Olsson, P. Tunestål, B. Johansson, S. Fiveland, R. Agama, and M. Willi. Compression ratio influence on maximum load of a natural gas fueled HCCI engine. In *SAE World Congress*, 2002. SAE 2002-01-0111.

[8] L. Koopmans, O. Backlund, and I. Denbratt. Cycle to cycle variations: Their influence on cycle resolved gas temperature and unburned hydrocarbons from a camless gasoline compression ignition engine. In *SAE World Congress*, 2002. SAE 2002-01-0110.

[9] C. S. Daw, R. M. Wagner, K. D. Edwards, and J. B. Green Jr. Understanding the transition between conventional spark-ignited combustion and HCCI in a gasoline engine. *Proc. of the Combustion Institute*, 31(2):2887–2894, 2007.

[10] D. Blom, M. Karlsson, K. Ekholm, P. Tunestål, and R. Johansson. HCCI engine modeling and control using conservation principles. In *SAE World Congress*, 2008. SAE 2008-01-0789.

[11] G. Särner, M. Richter, M. Aldén, A. Vressner, and B. Johansson. Cycle-resolved wall temperature measurements using laser-induced phosphorescence in an HCCI engine. In *Powertrain and Fluid Systems Conference and Exhibition*, 2005. SAE 2005-01-3870.

[12] L. Koopmans, H. Ström, S. Lundgren, O. Backlund, and I. Denbratt. Demonstrating a SI-HCCI-SI mode change on a Volvo 5-cylinder electronic valve control engine. In *SAE World Congress*, 2003. SAE 2003-01-0753.

[13] C.S. Daw, K.D. Edwards, R.M. Wagner, and Jr. J.B. Green. Modeling cyclic variability in spark-assisted HCCI. *J. of Engineering for Gas Turbines and Power*, 130(5):052801, 2008.

[14] A. Ghazimirsaied, M. Shahbakhti, and C.R. Koch. HCCI engine combustion phasing prediction using a symbolic-statistics approach. *J. of Engineering for Gas Turbines and Power*, 132(8):082805, 2010.

[15] G.M. Shaver and J.C. Gerdes. Cycle-to-cycle control of HCCI engines. In *ASME Int. Mechanical Engineering Congress and Exposition*, 2003. IMECE 2003-41966.

[16] D.J. Rausen, A.G. Stefanopoulou, J.-M. Kang, Eng J.A., and T.-W. Kuo. A mean-value model for control of homogeneous charge compression ignition (HCCI) engines. *J. of Dynamic Systems, Measurement and Control*, 3(3):355–362, September 2005.

[17] A. Widd, P. Tunestål, and R. Johansson. Physical modeling and control of homogeneous charge compression ignition (HCCI) engines. In *Proc. of the 47th IEEE Conference on Decision and Control*, pages 5615–5620, 2008.

[18] J. Bengtsson, M. Gäfvert, and P. Strandh. Modeling of HCCI engine combustion for control analysis. In *Proc. of the 43th IEEE Conference on Decision and Control*, volume 2, pages 1682–1687, 2004.

[19] G.M. Shaver, M.J. Roelle, and J.C. Gerdes. Modeling cycle-to-cycle dynamics and mode transition in HCCI engines with variable valve actuation. *Control Engineering Practice*, 14(3):213–222, 2006.

[20] K.L. Knierim, S. Park, J. Ahmed, A. Kojic, I. Orlandini, and A. Kulzer. Simulation of misfire and strategies for misfire recovery of gasoline HCCI. In *Proc. of the American Control Conference*, pages 3947–3952, 2008.

[21] C.G. Mayhew, K.L. Knierim, N.A. Chaturvedi, S. Park, J. Ahmed, and A. Kojic. Reduced-order modeling for studying and controlling misfire in four-stroke HCCI engines. In *Proc. of the 48th IEEE Conference on Decision and Control*, pages 5194–5199, 2009.

[22] C.J. Chiang, A. G. Stefanopoulou, and M. Jankovic. Nonlinear observer-based control of load transitions in homogeneous charge compression ignition engines. *IEEE Trans. Control Syst. Technol.*, 15(3):438–448, May 2007.

[23] C.J. Chiang and A. G. Stefanopoulou. Stability analysis in homogeneous charge compression ignition (HCCI) engines with high dilution. *IEEE Trans. Control Syst. Technol.*, 15(2):209–219, March 2007.

[24] J.-M. Kang. Sensitivity analysis of auto-ignited combustion in HCCI engines. In *SAE World Congress*, 2010. SAE 2010-01-0573.

[25] C. Wilhelmsson, A. Vressner, P. Tunestål, B. Johansson, G. Särner, and M. Aldén. Combustion chamber wall temperature measurement and modeling during transient HCCI operation. In *SAE World Congress*, 2005. SAE 2005-01-3731.

[26] C.S. Daw, M.B. Kennel, C.E.A. Finney, and F.T. Connolly. Observing and modeling nonlinear dynamics in an internal combustion engine. *Phys. Rev. E*, 57(3):2811–2819, 1998.

[27] C. J. Chiang and A. G. Stefanopoulou. Sensitivity analysis of combustion timing of homogeneous charge compression ignition gasoline engines. *J. of Dynamic Systems, Measurement and Control*, 131(1):014506, 2009.

[28] L. Manofsky, J. Vavra, D. Assanis, and A. Babajimopoulos. Bridging the gap between HCCI and SI: Spark-assisted compression ignition. In *SAE World Congress*, 2011. SAE 2011-01-1179.

[29] J.C. Livengood and P.C. Wu. Correlation of autoignition phenomena in internal combustion engines and rapid compression machines. In *5th Int. Symp. on Combustion*, volume 5, pages 347–356, 1955.

[30] Y. Mo. *HCCI heat release rate and combustion efficiency: A coupled KIVA multi-zone modeling study*. PhD thesis, University of Michigan, 2008.